

# Determining the depth and upwelling speed of the equatorial Ekman layer from surface drifter trajectories

Nathan Paldor<sup>1</sup> and Yair De-Leon<sup>1</sup>

<sup>1</sup>Fredy and Nadine Herrmann Institute of Earth Sciences  
Hebrew University of Jerusalem  
Edmond J. Safra Campus, Givat Ram, Jerusalem, 9190401 Israel

Correspondence to: N. Paldor ([nathan.paldor@mail.huji.ac.il](mailto:nathan.paldor@mail.huji.ac.il))

## Abstract

Trajectories of more than 500 drogued surface drifters launched since 1979 in the equatorial ocean are analyzed by employing the results of a new Lagrangian theory of the poleward transport from the equator forced by the prevailing Trade winds. The Lagrangian theory provides an explicit expression for the depth of the Ekman layer that circumvents the application of the 3-Dimensional continuity equation that requires calculating the divergence of horizontal transport, which was the basis of all previous studies on the subject. The analysis is carried out for drifters launched within 1° of the equator that reached final latitude of 3°, 4° or 5° North or South of the equator while remaining in one hemisphere throughout the entire travel time. The analysis yields robust estimates of 45 meters for the Ekman layer's depth and 1.0 m/day for the upwelling speed of thermocline water into the layer.

## 1. Introduction

The trade winds that blow westward in the Tropics due to action of the Coriolis force on the northerly surface winds of the Hadley circulation are the first and basic component of the heat transport from the warm equatorial surface ocean to the cold poles that mitigates the overall pole-to-equator temperature gradient on Earth. The mechanism that enables the poleward time-independent heat transport is the surface flow in the ocean that is directed  $90^\circ$  to the right/left of the wind in the northern/southern hemisphere relative to the direction of the overlying wind. This counter-intuitive flow direction results from Earth's rotation that adds the Coriolis force to the stress applied by the winds at the ocean surface. This straightforward scenario of wind-driven ocean circulation appears in all textbooks (Knauss, 1996; Talley et al., 2011) but despite its convincing simplicity, currently, quantitative estimates of the parameters that control it vary widely depending on the data and method used in the calculations of these estimates.

The classical theory that describes the ocean response to forcing by the overlying winds was developed about 120 years ago by V.W. Ekman under the assumption of constant Coriolis frequency (Ekman, 1905). This assumption greatly simplifies the analysis by ensuring that all coefficients in the governing equations are constant. The dynamics described in Ekman's theory includes a steady flow perpendicular to the wind direction and inertial, i.e. force-free, oscillations at the local (constant) Coriolis frequency. This is in sharp contrast to the equatorial region where the Coriolis frequency vanishes at the equator and varies (linearly) with latitude, which turns the equations nonlinear so the oscillation-free flow is not steady as in Ekman's original mid-latitude theory. The poleward directed surface flows in both hemispheres along the equator imply a strong horizontal divergence along the equator which can only be balanced by the upwelling of deeper water into the wind-forced, Ekman, layer. Though the heuristic application of the mid-latitude Ekman theory to the vicinity of the equator is quite straightforward, to-

date, it could not be employed to estimate either the depth of the equatorial Ekman layer or the rate of upwelled volume of water.

The complications that result from the inclusion of the meridional variation of the Coriolis frequency in Ekman's theory were recently resolved in a theory of wind-driven flow in which Ekman's 1905 classical theory was extended to the equatorial region (Paldor, 2024). This new theory employs the adiabaticity method (Goldstein, 1980; Paldor and Friedland, 2023) that filters out fast oscillatory dynamics from the slow dynamics associated with the motion of the center of oscillation. In the context of the equatorial Ekman problem the eliminated oscillations result from the meridionally varying Coriolis force while the slow and monotonic poleward motion results from the combination of the wind stress and the Coriolis force. The essence of the method is the formulation of the problem as the dynamics of a (quasi-)particle about the minimum of a potential while the potential itself varies with time on a slower time scale than the period of oscillations about the minimum. The potential is derived from the meridional Lagrangian momentum equation when the zonal velocity,  $U$ , is expressed as  $U = D + \int f(y)dy$  where  $f(y)$  is the latitude-dependent Coriolis frequency ( $= \beta y$ ) and  $D$  is the pseudo angular momentum, which is conserved in the absence of other (body) forces. The substitution of the angular momentum for the zonal velocity is essential for the analysis in spherical coordinates RomKedar et al. (1997). Additional details of the theory are given in Sect. 2.1.

Direct observations of the depth (thickness) of the equatorial Ekman layer and the rate of upwelling water to it are difficult to quantify due to the poor observational definition of the layer's dimensions and the extremely low speed of upwelling. Halpern and Freitag (1987) and Johnson et al. (2001) estimated the upwelling rate in the equatorial Pacific Ocean above 50 m depth to be about 2 m/day from the divergence of several moored horizontal current meters. Below 50 m depth their estimated vertical velocity is negative (directed downward). A similar upwelling rate of 2 m/day extending to depths of 120 m was estimated by Halpern et al. (1989) between 110°W and 140°W from December 1983 – September

1984 (but excluding April 1984) using the same method of inferring vertical speeds from the divergence of horizontal currents measured by moored current meters. The upwelling speed decreased eastward in these observations and the variation of the observed values greatly exceeded the mean values. In the same region (Central Pacific) but in February 1980 – March 1980 Bubnov (1989) used a similar method of integrating the 3D continuity equation associated with observed horizontal currents, and estimated the upwelling velocity over the upper 300 m to vary between 1 and 8 m/day.

Surface drifter trajectories deployed in the Eastern Pacific during 1977-1982 were used by Hansen and Paul (1987) as proxies of the currents and the trajectory divergence as a proxy of the current's divergence, which yielded an upwelling speed of 1.5 m/day in a stripe of  $\pm 1.5^\circ$  of the equator. The idea underlying their analysis is that the drifter trajectories represent the currents and divergence in the top 50 m. As noted by the authors, the main issue with their analysis is the accuracy of representation of currents by drifter trajectories. Using over 700 drifters launched between 1979 and 1990 Poulain (1993) estimated an upwelling velocity of 15 – 20 m/day between  $90^\circ\text{W}$  and  $150^\circ\text{W}$  in the equatorial Pacific. The method used by Poulain (1993) in the interpretation of drifter observations is to average the drifter velocities in given geographical domains and at selected time intervals to generate the Eulerian velocities at the center of the domain at that time. The high values of upwelling velocity in this study result from the small areas used for inverting the observed Lagrangian drifter velocities to Eulerian fields. Two important conclusions emerge from that study: The first is that except for its western part, the horizontal divergence in the equatorial Pacific is quite uniform and therefore so should be the upwelling speed. The second is that the upwelling velocity decreases monotonically with the assumed width of the meridional band over which the horizontal divergence is calculated.

Estimates of upwelling rates were also calculated based on the distribution of  $^{14}\text{C}$  released in large amounts to the atmosphere between 1955 and 1963 when above-ground nuclear tests took place. An analysis of the oceanic uptake of  $^{14}\text{C}$  and its redistribution in the Pacific Ocean carried out by Quay et al.

(1983) yielded a value of about 0.3 m/day for the upwelling velocity along the equator. Aside from this geo-isotopic study the previous estimations of the horizontal divergence fields were obtained either directly from current meter observations or indirectly from drifter trajectories. In the latter case that data were either spatially averaged to yield the Eulerian fields or interpreted as proxies of these fields. In contrast, the current study applies a recently developed Lagrangian dynamical theory directly to observed drifter trajectories which bypasses the need to estimate first the horizontal divergence. The large number of drifters, the accurate tracking of their location by satellites and the longtime of coverage allows for a selection of sufficient number of drifter trajectories that satisfy pre-determined selection criteria and yields accurate estimates of the depth of the equatorial Ekman layer and the speed of upwelling into it.

The application of the Lagrangian theory to drifter observations and the data used in this study are detailed in Section 2. In Section 3 we give the results obtained by applying the theory to drifter trajectories and the study is summarized in Section 4.

## **2. Theory and Data**

### **2.1. Theory**

The recent extension of the wind-driven theory of ocean circulation to the equator described in Paldor (2024) has demonstrated that, as in Ekman's original theory, the oceanic response can be decomposed into a monotonic, slow, flow (which is directed poleward in the equatorial region) and fast, large amplitude, oscillations. In contrast to Ekman's original theory, in the equatorial region when the wind stress is directed westward the oscillations are highly nonlinear and of large amplitude. An example of the large amplitude inertial oscillations associated with an initial impulse of a westward directed velocity when no wind stress affects the motion is shown in Fig. 1a. The present study applies the explicit expressions developed in Paldor (2024) to the observed trajectories of surface drifters and employs the

122 nondimensional variables and parameters in Eq. 10 of Paldor (2024). The dimensional counterpart of this  
 123 equation is:

$$124 \quad \frac{dy}{dt} = \frac{1}{y(t)} \frac{-\tau^x}{H} \left( \frac{R_e}{2\Omega\rho} \right). \quad (1)$$

125 Here,  $y(t)$  is the distance from the equator at time  $t$ . The global parameters in this relation are:  $\rho =$   
 126  $1027 \text{ kg m}^{-3}$  (water density),  $\Omega = 7.29 \cdot 10^{-5} \text{ s}^{-1}$  and  $R_e = 6371 \cdot 10^3 \text{ m}$  (Earth's rotation frequency  
 127 and radius, respectively) so  $\left( \frac{R_e}{2\Omega\rho} \right) = 4.25 \cdot 10^7 \text{ m}^4 \text{ s kg}^{-1}$ . The remaining, particular, parameters are:  $\tau^x$   
 128 - the wind stress (units:  $\text{N m}^{-2}$ ; negative for easterly winds) and  $H$  (m) - the Ekman layer's depth.

129 Multiplying the nonlinear relation (1) by  $y(t)$  and integrating the resulting 1<sup>st</sup> order equation for  $y(t)^2$   
 130 yields:

$$131 \quad y(t)^2 = y(0)^2 + 2 \frac{-\tau^x}{H} \cdot \left( \frac{R_e}{2\Omega\rho} \right) t. \quad (2)$$

132 As demonstrated in Fig. 1, this expression (shown by the red curve) successfully filters out the inertial  
 133 oscillations from the actual latitude time-series (blue curves), and describes the net, oscillation-free,  
 134 poleward motion.

135 Inverting Eq. (2) to an explicit expression for  $H$ , setting  $t$  to  $t_i$ , the travel time of drifter  $\#i$ , and  $y(t)$  to  
 136  $L$ , a “boundary” of the equatorial region, yields the estimate of  $H_i$  the depth value based on trajectory  $\#i$ :

$$137 \quad H_i = \left( \frac{R_e}{2\Omega\rho} \right) \frac{2(-\tau^x)}{L^2 - y_i(0)^2} t_i, \quad (3)$$

138 where  $y_i(0)$  is the distance of drifter  $\#i$  from the equator at  $t = 0$  (i.e. the distance of the launch point  
 139 from the equator).

## 140 2.2. Drifter trajectories

141 Nearly 30,000 surface drifters were released from 1979 at the ocean surface (Lumpkin et al., 2017) and  
 142 the geographical trajectories of these drifters are tracked by satellites every 6 hours for periods of up to

1000 days. These (Lagrangian) observations cover the global ocean and a few percent of them were launched on both sides of the equator in the Pacific, Atlantic and Indian oceans. The slightly negatively buoyant drifter is typically drogued at 15-meter depth, so it provides an estimate of the current in the top 15 meters of the water column where the wind stress is the primary forcing (Lumpkin et al., 2017). The agreement between drifter trajectories and ocean currents demonstrated in Lagerloef et al., (1999) and assumed in Poulain (1993) motivates an analysis of observed drifter trajectories in order to determine the depth of the equatorial Ekman layer and the upwelling speed of deep water into it.

The drifter trajectories used in the analysis are freely available from NOAA Global Drifter Program (NOAA/AOML/GDP) site. The data were screened according to the following three criteria:

1. They were launched within  $1^\circ \approx 110$  km south or north of the equator (regarded as the equator).
2. Once launched, the drifters remained in one hemisphere throughout the entire travel time to the final latitude (this is because equator crossing is not possible under the assumed westward directed wind stress).
3. The drifters were continuously tracked, with gaps no longer than one day, during their motion from the launch point to the final latitude that marks the boundary of the equatorial region (i.e.  $3^\circ \approx 330$  km,  $4^\circ \approx 440$  km or  $5^\circ \approx 550$  km).

The latitudes  $3^\circ$  and  $4^\circ$  were used in previous studies to define the boundaries of the equatorial region (Brady and Bryden, 1987; Lagerloef et al., 1999; Johnson et al., 2001) but in the present study we also used  $L = 5^\circ \approx 550$  km to verify the robustness of the calculated averages to the selected values of  $L$ .

The case  $L = 2^\circ$  is not included in the analysis since the singularity of Eq. (3) at  $L^2 = y_i(0)^2$  affects the accuracy of the estimates of  $H_i$  when  $L$  is close to  $y_i(0)$  i.e. for  $L = 2^\circ \approx 220$  km and for  $y_i(0) \leq 1^\circ$  the denominator is tiny which can yield extremely high value of  $H_i$  and amplify observational errors.

As of August 2024 ~30,000 drifter trajectories are archived in AOML archive and over 1500 drifters were launched near the equator and reached the final latitudes of  $3^\circ$ ,  $4^\circ$  or  $5^\circ$ , out of which ~700 drifters

remained in one hemisphere. The number of drifters in the Atlantic and Pacific oceans that reached each of the final latitudes is given in the 2<sup>nd</sup> column of Table 1 that also gives the mean  $y_i(0)$  ( $\equiv Y(0)$ , 3<sup>rd</sup> column) and the mean  $t_i$ , ( $\equiv T$ , 4<sup>th</sup> column) to the final latitudes (noted in the rows of this table). The Indian Ocean is excluded from the analysis due to the positive mean annual wind stress in it (see Sect. 2.3). No screening was made of drifters that lost their drogues on their way from  $y_i(0)$  to  $L$ .

### 2.3. Wind stress

The daily wind stress values over the oceans,  $\tau^x$ , used in this work are available at NOAA/CoastWatch site in 0.125° spatial resolution for 1999 – 2009. We calculated the averaged wind stress for the whole period in the entire region of the Indian, Atlantic and Pacific oceans in a zonal strip that straddles the equator between  $-L$  and  $+L$ , where  $L$  corresponds to 3°, 4° or 5°.

$L$ (degrees)	Number of drifters	Mean $y_i(0)$ (degrees)	Mean $t_i$ (days)	$\tau^x$ ( $Nm^{-2}$ )	Mean $H_i$ (m)	$W = \frac{H}{T} \cdot \frac{L-Y(0)}{L}$ (m/day)
3.04	610	0.29	29.67	-0.0261	51.10	1.56
4.04	576	0.29	43.43	-0.0264	42.48	0.91
5.04	531	0.29	58.12	-0.027	37.16	0.60

**Table 1: Drifter characteristics in the Pacific and Atlantic oceans and the zonal wind stresses there. The shown values of  $L$  are larger by a few kilometers compared to the distances corresponding to 3°, 4° or 5° since a drifter is determined to be “at  $L$ ” with an offset of up to 6 hours after its passage of that point. Less than 10% percent of the relevant drifters were launched in the Indian ocean which is not included in this table and in the analysis since the annual mean wind stress in the Indian Ocean is directed eastward, which is inconsistent with a poleward directed net motion. The 5<sup>th</sup> column denotes the mean wind stress daily values over the entire 1999 – 2009 period in each ocean used in this study. The variables  $H, T$  and  $Y(0)$  denote the mean values (over all drifters) of  $H_i, t_i$  and  $y_i(0)$ , respectively.**

These wind stress averages are given in the 5<sup>th</sup> column of Table 1 for the Atlantic and Pacific oceans, where the values are nearly identical (they differ by no more than a few percentage points) but not for the Indian ocean where the calculated mean values of the wind stress are positive (so  $H_i < 0$ ) and small



(less than  $+0.01 \text{ N m}^{-2}$ ) probably due to the strong seasonal forcing by the Monsoon system that induces eastward directed zonal winds throughout part of the year in this ocean (Hastenrath and Polzin, 2004; Zhang et al., 2022). The decade-long zonal wind stress observations are considered representative of the climatic values that prevailed throughout the trajectories of all drifters. Though the negative mean temporal values of  $\tau^x$  in the Atlantic and Pacific Oceans are not spatially uniform (reaching their maximal values in the center of each ocean and tapering off near the continents that bound the ocean on the east and west sides) only the spatially mean values are used.

### 3. Results

Four representative drifter trajectories are shown in Fig. 2 and they demonstrate the richness of observed trajectories near the equator, the intricate combination of oscillations with slow poleward propagation and the occurrence of equatorial crossing in many trajectories.

Substituting the values of  $y_i(0)$  and  $t_i$  for each drifter in Eq. (3) yields the corresponding values of  $H_i$ . The 6<sup>th</sup> column of Table 1 gives  $H$ , the mean of the particular values of  $H_i$ , and the histograms of the  $H_i$  values for each value of  $L$  are shown in Fig. 3 so the value of  $H$  is best estimated by:  $H = 44 \pm 7 \approx 45 \text{ m}$ .

Equation (2) can also be employed to calculate the poleward, oscillation-free, velocity of a drifter on its way from  $y_i(0)$  to  $L = y(t_i)$  from the drifter's average speed during its travel:  $V_i = \frac{L - y_i(0)}{t_i}$ . Thus, the volume divergence (per unit length in  $x$ ) that results from the anti-parallel, poleward directed, volume fluxes of 2 water columns that are initially conjoined along the equator and move poleward is  $2H_i V_i = 2H_i \frac{L - y_i(0)}{t_i}$ . The vertical volume flux (per unit length) due to Ekman upwelling during  $t_i$  is:  $2LW_i$ , where  $W_i$  is the upwelling speed. Equating the vertical and horizontal fluxes yields  $W_i L = H_i \frac{L - y_i(0)}{t_i}$  or  $W_i = \frac{H_i}{L} \frac{L - y_i(0)}{t_i}$ . The mean values of  $H_i$  and  $t_i$  in Table 1, denoted by  $H$  and  $T$ , then yield the mean values of  $W$  in the 6<sup>th</sup> column that averages to  $W \approx 1.0 \text{ m/day}$  for the three values of  $L$ .

The estimated  $H$  and  $W$  values along the equatorial Atlantic and Pacific Oceans are noted in Fig. 4 on a qualitative, textbook, cartoon of the wind forcing and resulting oceanic flow patterns.

#### 4. Summary and Discussion

The mean estimates of  $H = 45 \text{ m}$  and  $W = 1 \text{ m/day}$  calculated here based on surface drifter trajectories are more robust compared to prior estimates derived from standard hydrographic observations. Table 1 shows that the present estimates of  $H$  vary with  $L$  by a few meters and those for  $W$  by about  $0.5 \text{ m/day}$ . These variations are smaller than those of estimates based on standard hydrographic data that can vary by about one order of magnitude (Wyrski, 1981; Brady and Bryden, 1987; Lukas and Lindstrom, 1991; Weingartner and Weisberg, 1991). As an example, the  $H = 45 \text{ m}$  value reported here exceeds the estimate of 30-40 m proposed in Lukas and Lindstrom (1991) but the  $O(10\%)$  variation of the present estimate is significantly smaller than the  $O(80\%)$  variation in the previous estimate. In view of the crucial role played by the poleward flow of warm equatorial water in mitigating the large radiative pole-to-equator temperature gradient (Czaja and Marshal, 2006; Hartmann, 2016) a reliable quantification of the initiation of this flow is important for understanding Earth's climate.

The zonal stress is not uniform, reaching a maximal value in the center of the Ocean and tapering off towards the boundaries on the east and west. The effect of this variation on the value of  $H$  is pronounced in the equatorial Pacific Ocean and calculations of  $H$  using the values of  $\tau^x$  at each drifter's initial location, yield a wider range of  $H$  values. These estimates, too, are not exact since the value of  $\tau^x$  varies with time and along the drifter trajectory. A detailed analysis of the variation of  $\tau^x$  along a drifter trajectory and its effect on the value of  $H_i$  calculated in that trajectory are left for future work.

In contrast to Ekman's theory in mid-latitude, the extension of this theory to the equatorial region implies that the slow net poleward motion of a water column subject to a zonal wind stress is accompanied by a zonal component. This results naturally from the inertial oscillations that involve net

234 zonal translation on the equator (as in Fig. 1a), while inertial oscillations on the mid-latitudes  $f$ -plane are  
235 not accompanied by a translatory motion.

236 The results calculated in Sect. 3 focus on the net poleward propagation rate, which neglects the  
237 inertial oscillations, while the observed trajectories include both types of motion. The neglect of inertial  
238 oscillations in the observed trajectories is justified based on the fact that the period of these oscillations is  
239 much shorter than the temporal length of the averaged trajectory used for calculating  $H_i$  in Eq. (3). The  
240 high variability of the geographical trajectories, which is exemplified in Fig. 2, does not permit an estimate  
241 of the oscillations' period directly from the trajectories. However, for the values of  $\tau^x = 0.026 \text{ Nm}^{-2}$  and  
242  $H = 45 \text{ m}$  the period of inertial oscillations can be estimated from the scale  $P = \left( \beta \cdot \frac{\tau^x}{\rho H} \right)^{\frac{1}{3}} \approx 5 \text{ days}$   
243 which is much shorter than the typical 30-60 days trajectory length (see the values of mean  $t_i$  in Table 1).  
244 Thus, during the relatively long drifter travel time the poleward motion due to the oscillations averages  
245 out to zero, leaving the poleward motion of the oscillations' centers as the sole contributor to the net  
246 motion.

247 The results shown in Table 1 imply a decrease in the value  $H$  (and hence the value of  $W$ ) with the  
248 increase in  $L$ . This result is not trivial since Eq. (3) is also satisfied with constant  $H_i$  provided  $L^2 \propto t_i$  for  
249  $y_i(0) \ll L$ . However, the calculated values of mean  $t_i$  for different values of  $L$  reported in Table 1 only  
250 show a power slightly above 1.0 but significantly smaller than 2.0. The variation of  $H$  with  $L$  probably  
251 originates from a mechanism similar to that depicted by the blue arrows in Fig. 4b where the depth of the  
252 Ekman layer becomes shallower with the distance from the equator, which affects the relation between  $T$   
253 and  $L$ . The suggested mechanism is reminiscent of the thinning of smoke billows far from the smoke stack  
254 but we note that the transition from Eq. (1) to Eq. (2) is valid only when  $H$  is independent of  $t$  and  $y$ .

255 Though no explanation is proposed here for the quantitative dependence of  $H$  on  $L$  this result is  
256 consistent with the results reported in Fig. 3 of Poulain (1993), which show that the horizontal divergence

decreases monotonically with the width of the latitudinal band. We also note that Eulerian calculations of  $\frac{\partial v}{\partial y}$  based on spatial averaging of the Lagrangian observations as was done in Poulain (1993) yield an estimate of  $W/H$  so additional information is needed for determining each of these parameters (Poulain, 1993 arbitrarily assumed  $H = 50$  m). In contrast, in the present study  $H$  is determined directly from drifter trajectories, which yields an estimate of  $W$  based on mass conservation in a box of meridional extent  $2L$ , thickness  $H$  and unit zonal length.

The successful application of the new dynamical theory of wind-driven equatorial transport in the ocean developed in Paldor (2024) lends credence to the relevance of this theory to observations in the equatorial ocean and in particular to the use of the velocity at 15 m as representative of the surface Ekman layer. This relevance is demonstrated despite the omission of important factors such as the meridional wind stress (can be significant at short times), the initial drifter velocity (assumed to vanish in the theory) or the spatial and temporal changes of the zonal wind stress. It can be argued that the calculation and successful application of the oscillation-free speed of poleward wind-driven motion on the equator is of similar significance to ocean dynamics as the development of the expression for the steady transport in the original  $f$ -plane Ekman theory.

#### **Author contribution:**

NP: Initiation of project, writing various drafts and theoretical analysis.

YD: Data collection and analysis, editing and production of display items.

**Competing interests:** The authors declare that they have no conflict of interest.

**Financial support:** The authors happily declare that no funding was received for this study

278 **Data Availability:** The drifter data used in this study are maintained by NOAA/AOML and the  
279 wind stress data are maintained by NOAA/CoastWatch, both sites are noted in the list of  
280 references

281 **Acknowledgements:** The authors are grateful to two anonymous reviewers whose comments  
282 greatly improved the presentation of this paper.

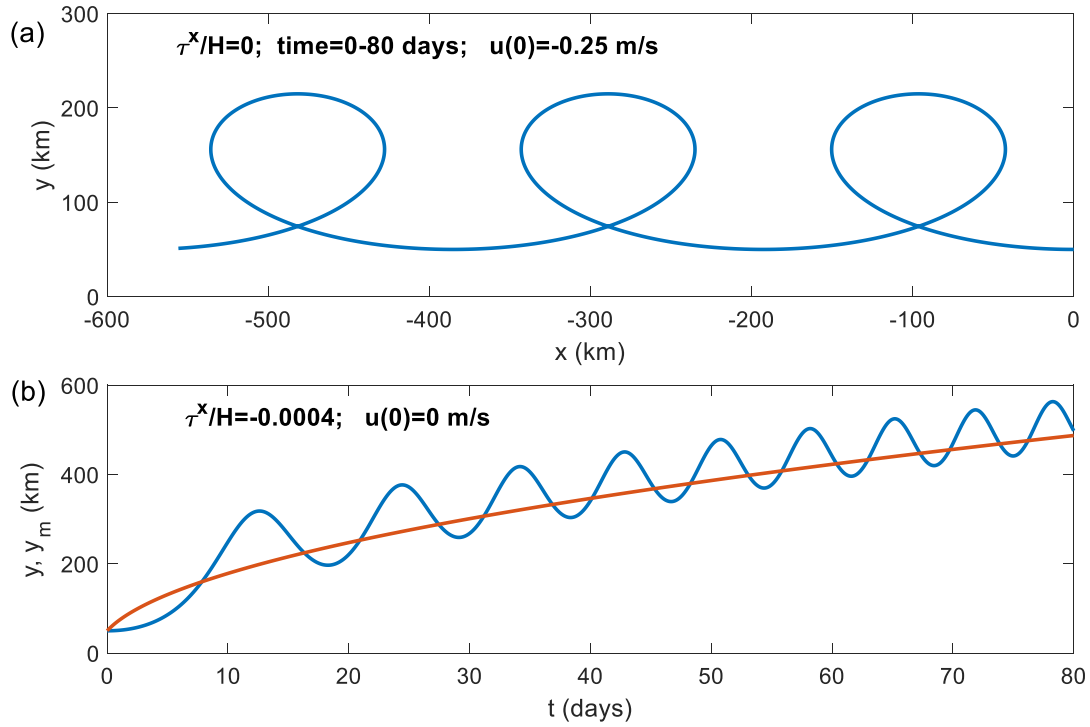
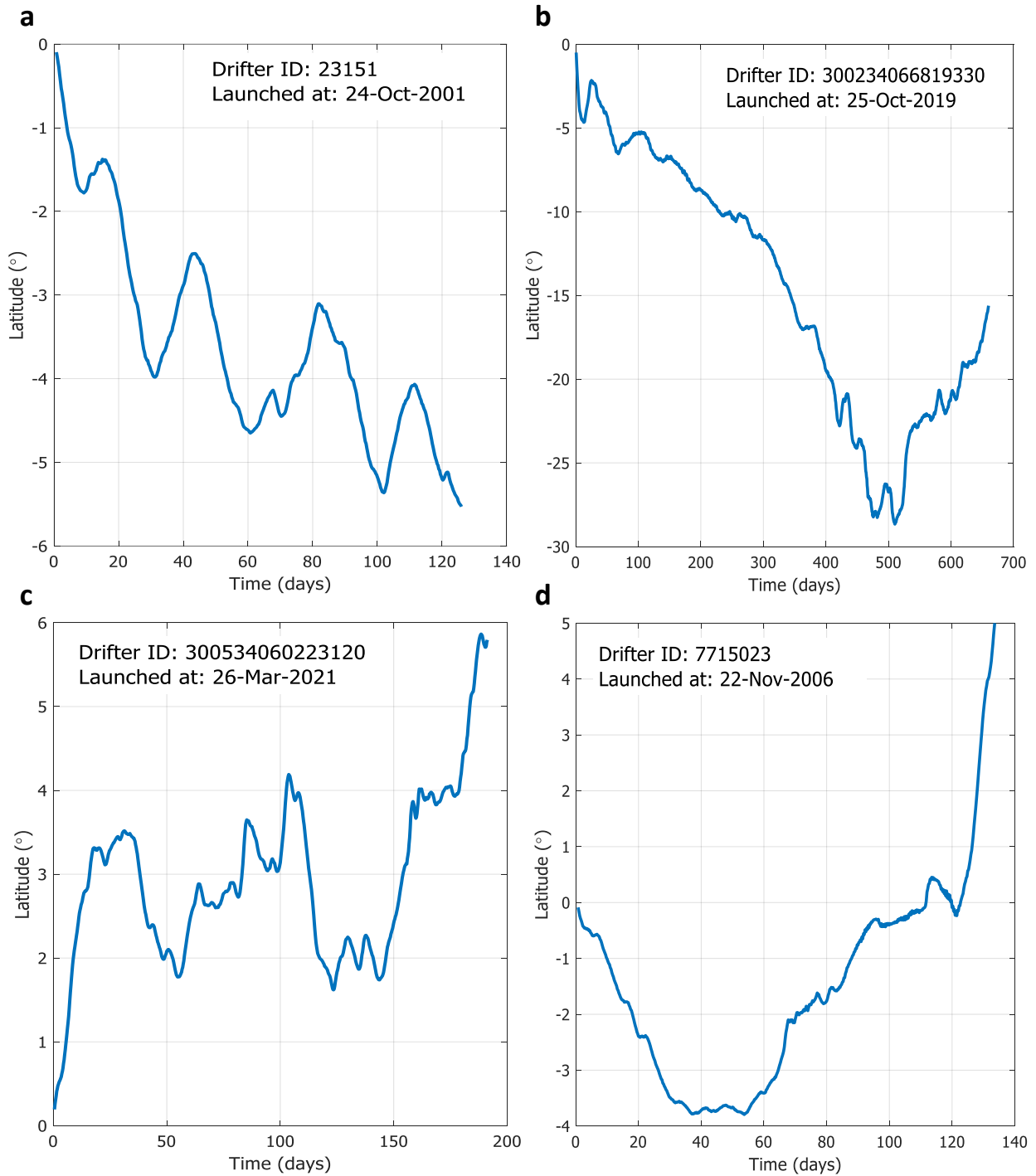
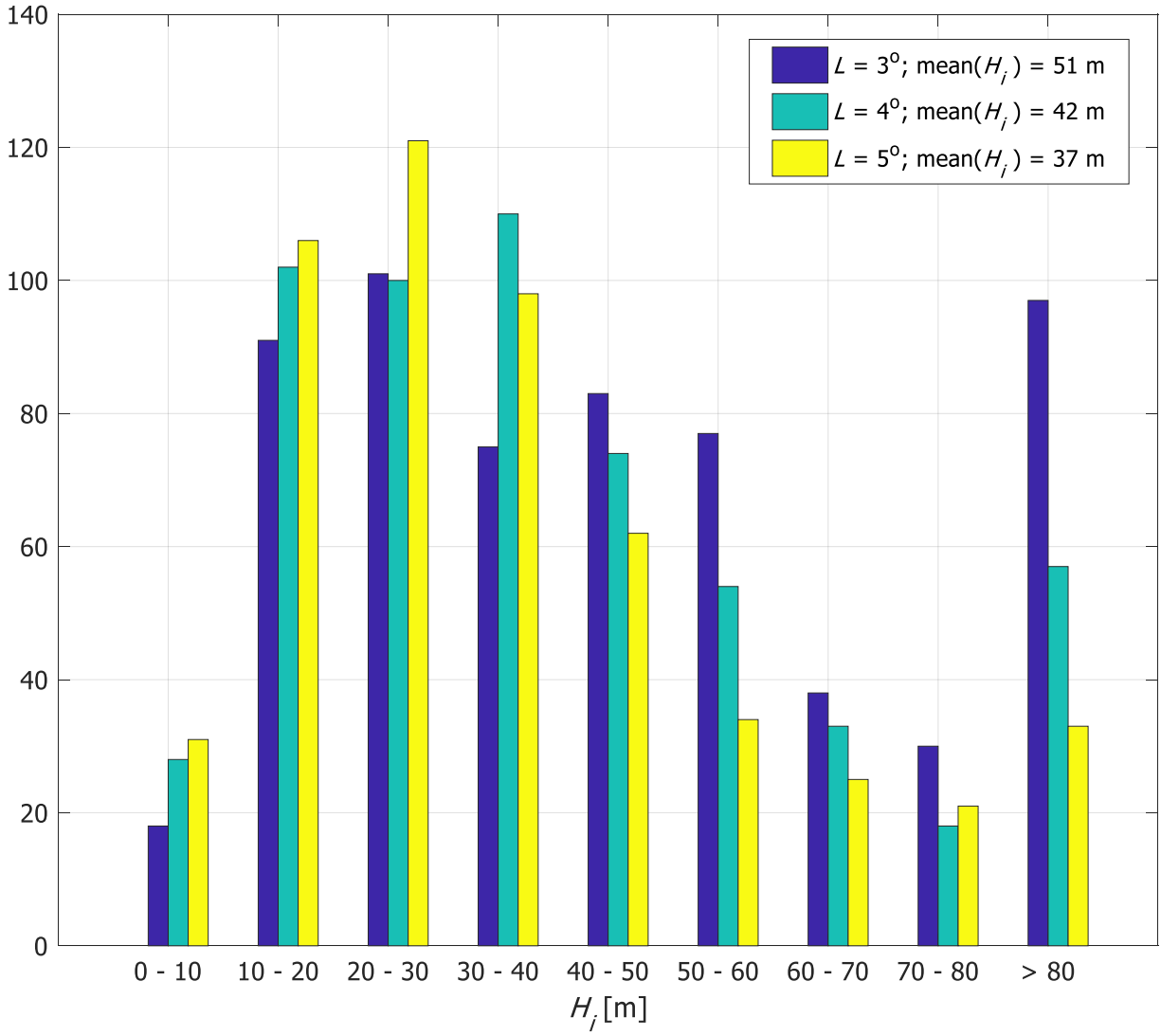


Figure 1: Panel (a): The numerically calculated geographic trajectory of a water column initiated with a westward directed impulse of  $0.25 \text{ m s}^{-1}$  zonal velocity subject only to the, latitude-dependent, Coriolis force. Panel (b): the latitude (i.e. distance from the equator in km) time-series (blue curve) and the oscillation free latitude time-series given by Eq. (2) denoted here by  $y_m$  (red curve) of a 50 m deep water column forced by a westward directed wind stress,  $\tau^x$ , of  $0.02 \text{ N m}^{-2}$ . In both panels the initial distance from the equator is  $y(0)=50$  km while the initial longitude and the initial meridional velocity are both 0.



**Figure 2: Four drifter trajectories originating within 1° of the equator analyzed in this study. a) A typical southern hemisphere trajectory that clearly shows oscillations and a mean poleward flow; b) A fast southern hemisphere trajectory that reaches 4° in just a few days and remains operational for nearly 2 years; c) A slow northern hemisphere trajectory that reaches 4° in more than 100 days; d) Part of a trajectory that reaches 3° prior to crossing the equator so it is included in the analysis of  $L = 3^\circ$  but not in the  $L = 4^\circ$  or  $L = 5^\circ$  analyses since it reaches these latitudes only after crossing the equator.**



297

298 **Figure 3: The histograms of  $H_i$ -values for the 3 values of  $L$ . For  $L = 3^\circ$  the tail of  $H_i > 80$  m is as high**  
 299 **as the maximum cell of  $H_i = 20 - 30$  m consistent with singularity of Eq. (3) at  $L = y_i(0)$ .**



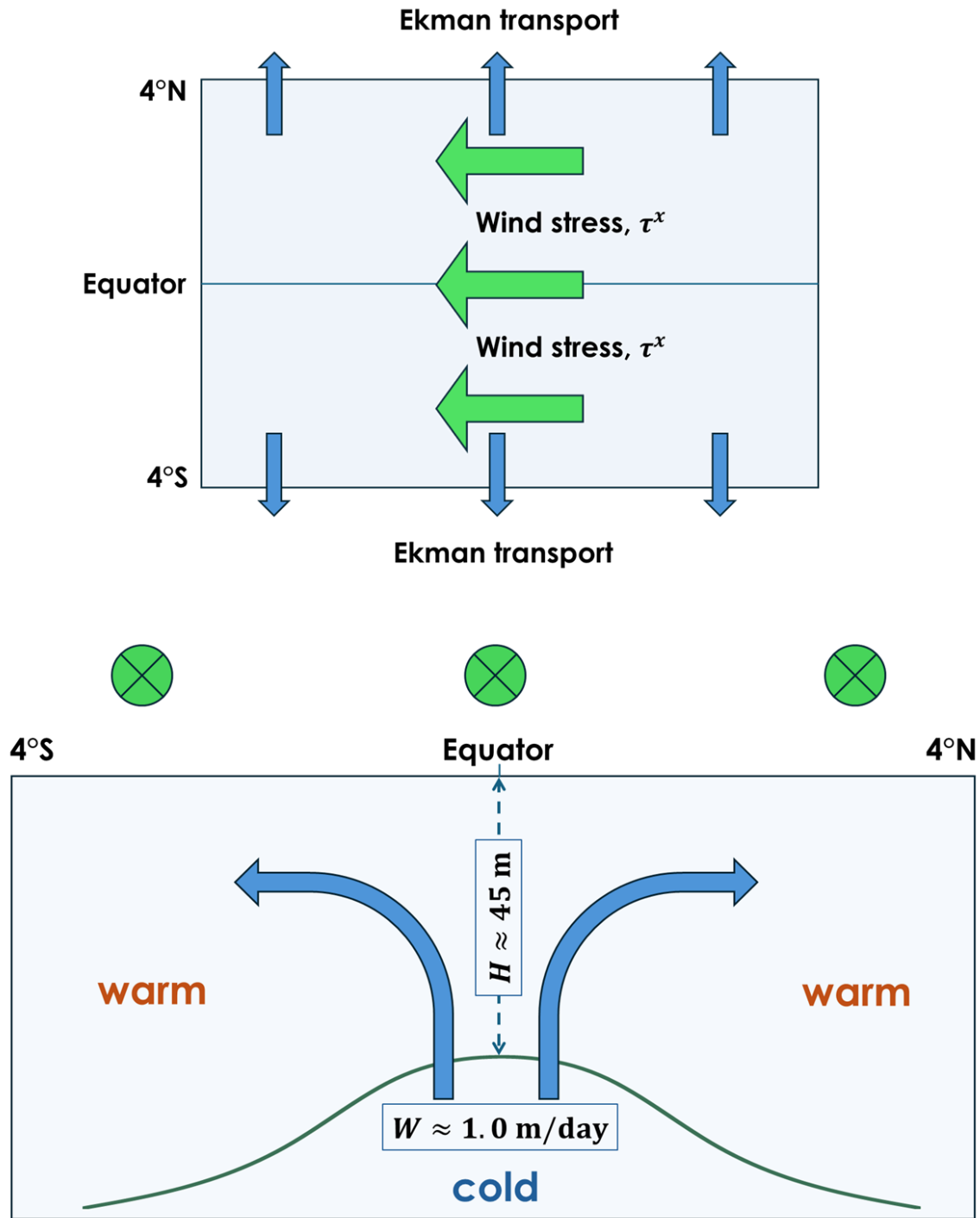


Figure 4: A sketch relating the poleward directed wind-driven surface flow along the equator under westward directed wind stress (upper panel – planar view) which is compensated by the upwelling of water from below (lower panel – latitude-height cross-section viewed from the east). The dark green curve in the lower panel denotes the boundary between the warm surface water and cold thermocline water. The  $H \approx 45 \text{ m}$  and  $W \approx 1.0 \text{ m/day}$  estimates are the main results of this study.

## References

- Bubnov, V. A.: Vertical motion in the Central Equatorial Pacific. *Oceanologica Acta, Special Issue*, Gauthier-Villars. 1987.
- Brady, E. C. and Bryden, H. L.: Estimating vertical velocity on the Equator. *Oceanologica Acta, Special Issue*, 1987.
- Czaja, A. and Marshall, J.: The partitioning of poleward heat transport between the atmosphere and ocean. *J. Atm. Sci.*, **63**(5), 1498-1511. <https://doi.org/10.1175/JAS3695.1>, 2006.
- Ekman, V. W.: On the influence of earth's rotation on ocean-currents. *Ark. Mat. Astr. Fys.*, **2**, 1–52, 1905.
- Goldstein, H.: *Classical Mechanics*. Addison-Wesley, Inc, 1980.
- Halpern, D. and Freitag, H. D.: Vertical motion in the upper ocean of the equatorial Eastern Pacific. *Oceanologica Acta, Special Issue*, Gauthier-Villars. 1987.
- Halpern, D., Knox, R. A., Luther, D. S. and Philander, S. G. H.: estimates of equatorial upwelling between 140° and 110°W during 1984. *J. Geophys. Res.:Oceans*. **94**(C6), 8018-8020. <https://doi.org/10.1029/JC094iC06p08018>. 1989
- Hansen, D. V. and Paul, C. A.: vertical motion in the Eastern equatorial Pacific inferred from drifting buoys. *Oceanologica Acta, Special Issue*, Gauthier-Villars. 1987.
- Hartmann, D. L.: *Global Physical Climatology*, 2<sup>nd</sup> Ed., Elsevier Inc. <https://doi.org/10.1016/C2009-0-00030-0>. 2016.
- Hastenrath, S. and Polzin, D.: Dynamics of the surface wind field over the equatorial Indian Ocean. *Q. J. R. Meteorol. Soc.*, **130**. 503-517. <https://doi.org/10.1256/qj.03.79>, 2004.
- Johnson, G. C., McPhaden, M. J., and Firing, E.: Equatorial Pacific Ocean Horizontal Velocity, Divergence, and upwelling. *J. Phys. Oceanogr.*, **31**(3), 839-849. [https://doi.org/10.1175/1520-0485\(2001\)031<0839:EPOHVD>2.0.CO;2](https://doi.org/10.1175/1520-0485(2001)031<0839:EPOHVD>2.0.CO;2), 2001.
- Knauss, J. A.: *Introduction to Physical Oceanography*, 2<sup>nd</sup> Ed. Prentice Hall, Inc. ISBN 0-13-238155-9, 1996.
- Lagerloef, G. S. E., Mitchum, G. T., Lukas, R. B. and Niiler, P. P.: Tropical Pacific near-surface currents estimated from altimeter, wind, and drifter data. *J. Geophys. Res.: Oceans*, **104**(10), 23,313-23,326. <https://doi.org/10.1029/1999JC900197>, 1999.
- Lukas, R. and Lindstrom, E.: The mixed layer of the western equatorial Pacific Ocean *J. Geophys. Res.: Oceans*. **96**, 3343-3357. <https://doi.org/10.1029/90JC01951>, 1991.
- Lumpkin, R., Ozgokmen, T. and Centurioni, L.: Advances in the application of surface drifters. *Ann. Rev. Mar. Sci.*, **9**, <https://doi.org/10.1146/annurev-marine-010816-060641>, 2017.
- NOAA/CoastWatch: <https://coastwatch.pfeg.noaa.gov/erddap/files/erdQStress3day/erdQStaux3day/>, last access: 22 September 2024.
- NOAA/AOM/GDP: [https://erddap.aoml.noaa.gov/gdp/erddap/tabledap/drifter\\_6hour\\_qc.html](https://erddap.aoml.noaa.gov/gdp/erddap/tabledap/drifter_6hour_qc.html), last access: 30 August 2024.
- Paldor, N. and Friedland, L.: Wind-driven transport of the spherical earth. *Phys. Fluids*, **35**, 056604. <https://doi.org/10.5194/os-19-93-2023>, 2023.

345 Paldor, N.: A Lagrangian theory of equatorial upwelling. *Phys. Fluids*, **36**, 046605.  
 346 <https://doi.org/10.1063/5.0202412>, 2024.

347 Poulain, P.-M.: Estimates of Horizontal Divergence and Vertical Velocity in the Equatorial Pacific. *J. Phys.*  
 348 *Oceanogr.* **23**, 601-607. 1993.

349 Quay, P. D., Stuiver, M. and Brocker, W. S.: Upwelling rates for the equatorial Pacific Ocean derived from  
 350 the bomb <sup>14</sup>C distribution. *J. Mar. Res.*, **41**, 769-792. 1983.

351 RomKedar, V. Dvorkin, Y. and Paldor, N.: Chaotic Hamiltonian Dynamics of particle's motion in the  
 352 atmosphere. *Physica. D*, **106**(3-4), 389-431. [https://DOI.org/10.1016/S0167-2789\(97\)00015-8](https://DOI.org/10.1016/S0167-2789(97)00015-8)

353 Talley, L. D., Pickard, G. L., Emery, W. J. and Swift, J. H.: *Descriptive Physical Oceanography: An*  
 354 *Introduction*, 6<sup>th</sup> Ed. Academic Press. ISBN: 978-0-7506-4552-2, 2011.

355 Weingartner, T. J. and Weisberg, R. H.: On the annual cycle of equatorial upwelling in the central Atlantic  
 356 Ocean, *J. Phys. Oceanogr.*, **21**(1), 68-82. [https://doi.org/10.1175/1520-](https://doi.org/10.1175/1520-0485(1991)021<0068:OTACOE>2.0.CO;2)  
 357 [0485\(1991\)021<0068:OTACOE>2.0.CO;2](https://doi.org/10.1175/1520-0485(1991)021<0068:OTACOE>2.0.CO;2), 1991.

358 Wyrski, K.: An estimate of equatorial upwelling in the Pacific. *J. Phys. Oceanogr.* **11**(9). 1205-1214.  
 359 [https://doi.org/10.1175/1520-0485\(1981\)011<1205:AEOEUI>2.0.CO;2](https://doi.org/10.1175/1520-0485(1981)011<1205:AEOEUI>2.0.CO;2), 1981.

360 Zhang, L., Li, Y. and Li, J.: Impact of equatorial wind stress on Ekman transport during the mature phase of  
 361 the Indian Ocean Dipole. *Clim. Dyn.* **59**, 1253–1264. <https://doi.org/10.1007/s00382-022-06183-7>,  
 362 2022.